

Chemical Approach Based ZnS-ZnO Nanocomposite Synthesis and Assessment of their Structural, Morphological and Photocatalytic Properties

Parita Basnet*, Dhruvajyoti Samanta, Somenath Chatterjee†

*Centre for Materials Science and Nanotechnology, Sikkim Manipal Institute of Technology,
Sikkim Manipal University, Sikkim, India*

(Received 12 January 2021; revised manuscript received 16 February 2021; published online 25 February 2021)

This work describes a comparative assessment between zinc oxide (ZnO) nanoparticles (NP), zinc sulfide (ZnS) NP and ZnS-ZnO nanocomposite (NC). A chemical non-aqueous method was chosen for materials synthesis. From XRD spectra, the crystalline phases and phase purity of the samples were confirmed. The average crystallite sizes were calculated as 69 nm, 5 nm and 10 nm for ZnO NP, ZnS NP and ZnS-ZnO NC, respectively, indicating a relatively pronounced growth and coarsening processes in ZnO NP. The lowering of band gap energy was verified through optical absorption spectra of ZnS-ZnO NC. Morphological investigation revealed that ZnO consisted of plate-like structures, ZnS comprised of agglomerated spheres while ZnS-ZnO NC exhibited both these structures. EDX and XPS spectra of ZnS-ZnO NC confirmed the presence of Zn, S and O in the NC. The photocatalytic degradation of cationic dyes were observed to be the highest by ZnS-ZnO NC compared to its individual components, ZnO and ZnS.

Keywords: ZnO nanoparticles, ZnS nanoparticles, ZnS-ZnO nanocomposite, XPS, Photocatalysis.

DOI: [10.21272/jnep.13\(1\).01025](https://doi.org/10.21272/jnep.13(1).01025)

PACS numbers: 61.72.Uj, 71.55.Eq, 78.40.Fy, 82.30.Lp

1. INTRODUCTION

ZnO and zinc sulfide (ZnS) are important II-VI semiconductors [4-9] containing earth-abundant elements and have been intensively studied for applications in UV-sensors, LASERS, field emitters, photocatalysis, etc. [10]. However, both possess large optical band gap energies of 3.3 eV and 3.67 eV [10], respectively, because of which, both these semiconductors are visible-light inactive. Hence, a limitation is imposed as far as the visible-light driven photocatalytic applications are concerned. Nevertheless, the heterostructure of ZnO and ZnS, i.e. ZnO coupled with ZnS, have enticed considerable theoretical and experimental studies since their couple develop a unique heterostructure possessing the photoexcitation threshold energy much smaller relative to the individual semiconductors [10-12].

Crystalline particles possessing high specific surface area are often synthesized in non-aqueous media which usually favors faster nucleation and growth processes compared to aqueous medium. Contrariwise, coarsening and oriented attachment may take place relatively slow in non-aqueous solvent and exhibit a huge impact on the particle size. During the supersaturation processes, ability to isolate nucleation and growth involving coarsening and oriented attachment is essential for eventually tuning the particle size. Hu et al. [1] reported zinc oxide (ZnO) nanoparticles (NP) synthesis using zinc salts in different alcoholic media with sodium hydroxide as the precipitant. They observed that nucleation and growth processes completed in the first several minutes of the reaction and the so-formed particles had an average particle diameter of 3 nm. Further, the Authors stated that the subsequent particle size increasing mechanism is directly reliant

on the system. Subsequent to nucleation and growth accomplishment, enlargement in size was found to be controlled and dominated by coarsening process, wherein, rate constant was found to depend upon the anion [2]. Additionally, these three processes were correlated to the chain length of the solvent alcohol [3]. Hu et al. [3] observed that although, nucleation and growth processes were slower in small alcohol chain (e.g. ethanol) as compared to longer chain alcohols (e.g. 1-hexanol), the process of coarsening and subsequent enlargement in the size of the particles were slower in the former as compared to the latter.

Considering these facts, in the present study, the synthesis of ZnO NP, ZnS NP and ZnS-ZnO nanocomposite (NC) were performed in ethanol medium. The as-synthesized NP and NC were then compared based on their optical, morphological and photocatalytic properties. The impact of ZnS semiconductor coupled with ZnO NC and the corresponding alteration in the visible-light induced photocatalytic efficiency of the individual components were mainly focused. The model dyes selected for this comparison were methylene blue (MB) and rhodamine B (RhB).

2. EXPERIMENTAL DETAILS

2.1 Chemicals and Instrumentation

Zinc acetate dihydrate $Zn(OAc)_2 \cdot 2H_2O$, Sodium hydroxide were procured from Loba Chemie. Methylene blue (MB) was purchased from Merck. Sodium Sulfide ($Na_2S \cdot 9H_2O$) and ethanol were Rankem made.

PANalytical Spectris technologies PW 3040/60 X-ray diffractometer with Cu $K\alpha 1$ radiation, working voltage of 40 kV and 30 mA current was used to ana-

* paritapyangs.pb@gmail.com

† somenath@gmail.com

The results were presented at the International Conference on Multifunctional Nanomaterials (ICMN2020)

lyze the X-ray Diffraction (XRD) pattern of the samples. UV-Vis absorption spectra were acquired using Shimadzu 1800 UV-Vis spectrophotometer within the scanning wavelength of 200-1100 nm. Morphological information was obtained using JEOL Field Emission Scanning Emission Microscopy (FESEM), Model: 7610F equipped with Energy Dispersive X-ray (EDX) analyzer.

2.2 Synthesis Procedure

For the synthesis of ZnO NP, 0.2 M $\text{Zn}(\text{OAc})_2 \cdot 2\text{H}_2\text{O}$ was dissolved in equal volumes of water and ethanol matrix. Similarly, 0.2 M NaOH solution was prepared in a similar manner. The two solutions were mixed and stirred for 4 h at 60 °C. The resultant was centrifuged, washed and dried at 80 °C for 4 h. For the synthesis of ZnS NP, 0.2 M $\text{Zn}(\text{OAc})_2 \cdot 2\text{H}_2\text{O}$ was dissolved in H_2O and ethanol matrix and similarly, another solution of Na_2S was prepared. Rest of the steps were similar to that of ZnO NP. For the synthesis of ZnS-ZnO NC, after mixing 0.2 M each $\text{Zn}(\text{OAc})_2 \cdot 2\text{H}_2\text{O}$ and NaOH in water-ethanol matrix, the resultant was stirred for 30 min at 60 °C. This was followed by the addition of 0.2 M Na_2S solution (prepared in water-ethanol matrix). The resulting solution was stirred for 4 h at 60 °C. Thereafter, the precipitate from the respective solutions were centrifuged, washed and dried at 80 °C for 4 h.

2.3 Procedure for Photocatalysis

50 mL RhB and MB solutions with an initial concentration of 5 μM were prepared. To this, 0.05 g of the respective photocatalyst added. The six solutions were then stirred vigorously for 30 min and then left undisturbed in dark condition. Thereafter, the solutions were exposed to visible light irradiation for 60 min. 5 mL of the supernatant containing the dye concentration from each of the solutions were then subjected to UV-Vis absorption measurements. The efficiency of the photocatalysts was estimated from equation 1.

$$\text{Degradation efficiency} = [(A_0 - A)/A_0] \times 100 \%, \quad (1)$$

where, A_0 and A are the initial and final absorbance at λ_{max} of MB dye.

3. RESULTS AND DISCUSSION

3.1 Sample Characterization

The XRD peaks of ZnO, ZnS and ZnS-ZnO NC have been indexed and the spectra are presented in Fig. 1. The diffraction pattern of ZnO displayed the characteristic peaks corresponding to that of wurtzite ZnO (JCPDS No. 36-1451), while that of ZnS represented the cubic phase (JCPDS No. 15-1691) [10]. In case of ZnS-ZnO NC, the pattern consists of diffraction peaks from ZnS and ZnO which have been differentiated using (*) and (#), respectively, in the figure. The decreased intensity of ZnS peak in ZnS-ZnO spectra indicated that the formation of ZnO tended to a lower crystallization of ZnS [10]. No shifts in the diffraction plane were observed indicating that ZnO and ZnS existed in

the coupled form. The average crystallite sizes of the as-synthesized NP and NC were calculated based on the Scherrer equation [8] and were found to be 69 nm for ZnO, 5 nm for ZnS and 10 nm for ZnS-ZnO NC. From these values, it may be concluded that the growth and coarsening processes in ZnO were more pronounced relative to that in ZnS and that the presence of ZnS nuclei in the growth medium of ZnS-ZnO hindered crystallite agglomeration.

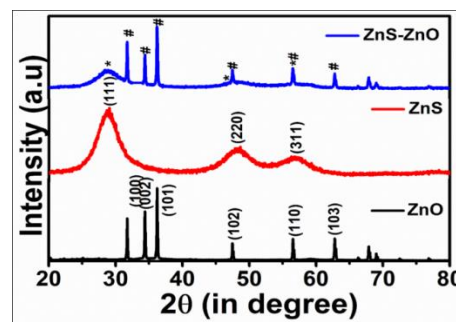


Fig. 1 – XRD spectra corresponding to ZnO, ZnS and ZnO-ZnS NC

Fig. 2 equates the optical absorption curves of as-synthesized ZnO, ZnS and ZnS-ZnO NC. The absorption maximum of ZnO and ZnS NP are located in the UV-region while that of ZnS-ZnO NC in the UV-Vis region. The corresponding band gap energies were estimated to be 3.4 eV for ZnO, 3.9 eV for ZnS and 3.2 eV for ZnS-ZnO NC. A hypsochromic shift was observed in case of ZnO and ZnS NP as compared to their bulk counterparts, which may be attributed to their nanometric size. Further, a bathochromic shift w.r.t as-synthesized ZnO and ZnS NP was observed in case of ZnS-ZnO NC. According to Literature, the coupling of ZnS and ZnO NP would activate their visible light absorption property as a consequence of increased number of surface defect centers and the development of surface granule-like layer structures that increases light scattering [13]. Thus, a similar explanation is valid in this case as well.

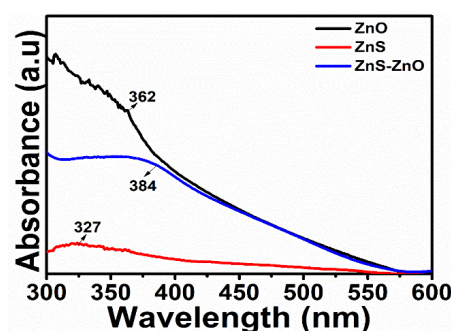


Fig. 2 – Absorption spectra of ZnO, ZnS and ZnS-ZnO NC

The surface morphology of the as-synthesized samples were studied through FESEM and Fig. 3 displays the results. The morphology of ZnO NP resembles continuous flake-like structure with enlarged particle size, as may be observed from Fig. 3 (a). On the other hand, FESEM image of ZnS (Fig. 3 (b)) shows the existence of very small spherical particles agglomerated to form longer extensions. These results are consistent with the

XRD results. The FESEM image of ZnS-ZnO NC, as shown in Fig. 3 (c), represents the existence of plate-like structure with irregular smaller particles, wherein, the former may be due to ZnO phase while the latter because of ZnS, based on their individual morphology. This further indicates that ZnO and ZnS exists as individual phases. Fig. 3 (d) corresponds to the EDX spectra of ZnS-ZnO NC. It may be observed from the percentage composition that the weight percentage of S and O are approximately similar in this NC. Please note: Au spectral lines are observed in the EDX spectra because of gold-coating done on the sample prior to FESEM analysis.

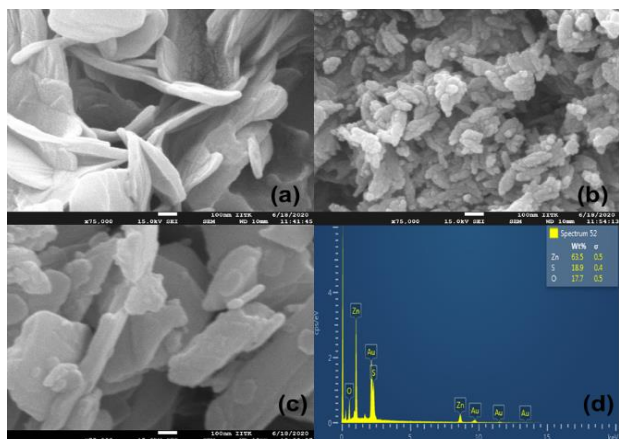


Fig. 3 – FESEM micrographs of (a) ZnO, (b) ZnS, and (c) ZnS-ZnO, and (d) EDX spectra of ZnS-ZnO NC

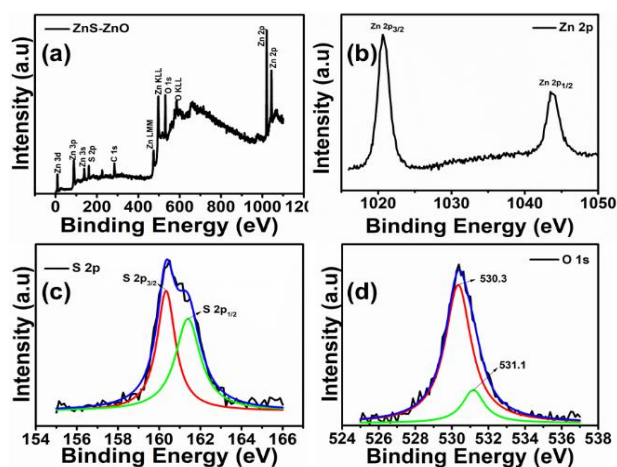


Fig. 4 – (a) XPS wide-survey spectra, (b) Zn 2p, (c) S 2p, and (d) O 1s of ZnS-ZnO NC

The chemical composition and oxidation states of the respective elements present in ZnS-ZnO NC were interpreted based on the results from XPS characterization that have been displayed in Fig. 4. The wide survey scan of ZnS-ZnO NC clearly represents Zn, O and S in the sample, in accordance with the EDX spectra. Two peaks at 1020.7 eV and 1043.5 eV for Zn 2p_{3/2} and Zn 2p_{1/2}, respectively, were observed for Zn, as may be seen in Fig. 4 (b), which are in agreement with the earlier reports [13, 14] and confirms the existence of Zn in ZnO and ZnS. Additionally, the Zn 2p doublet separation appears at 23-23.1 eV which further proves that Zn ions bind to S and O ions in ZnS and ZnO lattices, respectively [15]. The asymmetric S 2p peaks was de-

convoluted into two sub-peaks, as shown in Fig. 4 (c), which corresponds to S 2p_{3/2} at 160.3 eV and S 2p_{1/2} at 161.3 eV binding energies, representing the occurrence of S in ZnS [16]. The absence of S peak at binding energy value of ~162 eV corresponds to the non-existence of surface defects due to S-S species in ZnS [17]. Likewise, the asymmetric O 1s peak was deconvoluted into 530.3 eV and 531.1 eV components, as may be observed in Fig. 4 (d), which corresponds to the presence of O²⁻ in ZnO [18, 19].

3.2 Photocatalytic Studies

Fig. 5 shows the results of MB and RhB adsorption and photocatalytic degradation after 60 min of visible light irradiation by ZnO NP, ZnS NP and ZnS-ZnO NC. The adsorption and photocatalytic degradation efficiencies of the samples with the respective dyes have been presented in Table 1.

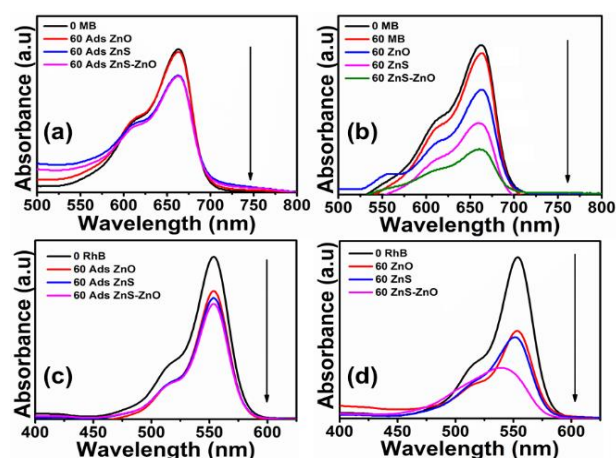


Fig. 5 – (a) Adsorption spectra of MB dye, (b) Degradation spectra of MB dye, (c) Adsorption spectra of RhB dye, and (d) Degradation spectra of RhB dye with ZnO, ZnS and ZnS-ZnO NC

It may be observed from Fig. 5 (a) that the adsorption of MB dye was the least for ZnO and comparable in case of ZnS and ZnS-ZnO NC. This observation may be ascribed to the larger particle size in the former as compared to the latter which consequently resulted in lower specific surface area in ZnO relative to ZnS and ZnS-ZnO NC. The photolysis of MB dye after 60 min of visible light irradiation did not produce any appreciable decrease in MB absorption maxima as seen in Fig. 5 (b). However, upon the addition of the as-synthesized samples, MB dye degradation was accelerated. The results of adsorption and photolysis indicates that light irradiation and presence of a photocatalyst are both equally important to effectively degrade the complex molecular structure of dyes.

Table 1 – Summary of the photocatalytic studies

Sample	% Adsorption in 60 min		% Degradation in 60 min	
	MB	RhB	MB	RhB
ZnO	2	21	29	46
ZnS	20	26	52	50
ZnS-ZnO	20	30	70	69

As far as the MB photocatalytic degradation efficiencies of the synthesized samples are concerned, it may be noted that least degradation was achieved with ZnO, followed by ZnS and maximum degradation was achieved with ZnS-ZnO NC as the photocatalyst. Thus, the coupling of two different semiconductor NM proved to be beneficial in terms of photocatalytic studies. Likewise, Fig. 5 (c) represents the adsorption spectra of RhB dye in the presence of the respective samples. As in the case of MB dye, the adsorption was found to be minimum in ZnO, intermediate in ZnS and highest in ZnS-ZnO NC. The degradation spectra, presented in Fig. 5 (d), entails that ZnS-ZnO NC exhibited the highest degradation efficiency as compared to their individual components. In both the cases of MB and RhB dye degradations, the inefficient action of ZnO and ZnS NP is understandable as both these NP absorb only UV-light, as was confirmed from their UV-Vis spectrum. However, in case of ZnS-ZnO NC due to the coupling of the two semiconductor NM, a bathochromic shift in the absorbance spectrum was observed which was tending to the visible region. As a consequence, the heterostructure of ZnS-ZnO NC was able to excite upon the action of visible light irradiation. Further, the recombination of exciton pairs is suppressed in ZnS-ZnO NC on account of their matching band position [20]. Therefore, visible light induced excitation of electron-hole pairs occurred in ZnS-ZnO NC, wherein, the photo-generated holes transferred from ZnO to ZnS promptly while photo-excited electrons on ZnS readily moved to ZnO because both VB and CB maxima of ZnO are higher than that of ZnS [20]. Consequently, the electrons on ZnO surface then interacted with adsorbed O₂ to form superoxide radicals which further reacted with H₂O and HO⁻ located on the surface of the photocatalyst to form hydroxyl radicals. These processes then led to the oxidation of organic dyes, MB and RhB, to form the degraded products. Meanwhile, holes in ZnS surface has the potential to directly oxidize the ad-

sorbed dye molecules. Thus, it may be concluded that the effective separation of the photo-generated exciton pairs was responsible for the superior photocatalytic efficiency of ZnS-ZnO NC as compared to their individual components.

4. CONCLUSION

The synthesis of ZnO and ZnS NP as well as their coupled NC was successful as was verified from the various characterization results. Interpretation of the XRD spectra led to the conclusion that both ZnO and ZnS NM were present as separate phases in the NC. UV-Vis absorption spectra revealed the visible-light active nature of ZnS-ZnO NC. From the FESEM images, formation of regular sheet-like structures was evident for ZnO NP, small sized spherical particles agglomerated with each other for ZnS NP and formation of irregular-plate like structure for ZnS-ZnO NC were revealed. The EDX spectra of ZnS-ZnO NC confirmed the existence of Zn, O and S in the sample with a similar weight percentage of O and S. XPS studies further confirmed the elemental composition of the as-synthesized NC. The enhanced photocatalytic degradation of two cationic dyes, MB and RhB, was observed with ZnS-ZnO NC as compared to individual ZnO and ZnS NP. This increase in photocatalytic degradation efficiency of the NC corresponds to its visible light activation and suppression of electron-hole pair recombination. Thus, ZnS-ZnO NC heterostructure may be considered as an effective visible light photocatalyst for MB and RhB dyes degradation.

ACKNOWLEDGEMENT

Ms. Parita Basnet is obliged for scholarship from Pai Endowment fund, Ref SMU/VC/2015-70, dated 17/11/2016.

REFERENCES

1. Z. Hu, D.J. Escamilla Ramirez, B.E. Heredia Cervera, G. Oskam, P.C. Searson, *J. Phys. Chem. B* **109**, 11209 (2005).
2. Z. Hu, G. Oskam, R.L. Penn, N. Pesika, P.C. Searson, *J. Phys. Chem. B* **107**, 3124 (2003).
3. Z. Hu, G. Oskam, P.C. Searson, *J. Colloid Interface Sci.* **263**, 454 (2003).
4. D. Samanta, T.I. Chanu, P. Basnet, S. Chatterjee, *J. Mater. Eng. Perform.* **27**, 2673 (2018).
5. P. Basnet, T. Inakhunbi Chanu, D. Samanta, S. Chatterjee, *J. Photochem. Photobiol. B Biol.* **183**, 201 (2018).
6. P. Basnet, T.I. Chanu, D. Samanta, S. Chatterjee, J. Mukherjee, *AIP Conf. Proc.* **2115**, 030204 (2019).
7. P. Basnet, S. Chatterjee, *Nano-Struc. Nano-Obj.* **22**, 100426 (2020).
8. P. Basnet, D. Samanta, T.I. Chanu, S. Jha, S. Chatterjee, *J. Mater. Sci. Mater. Electron.* **31**, 2949 (2020).
9. D. Samanta, P. Basnet, T. Inakhunbi Chanu, S. Chatterjee, *J. Alloy. Compd.* **844**, 155810 (2020).
10. H. Zhao, Y. Dong, P. Jiang, X. Wu, R. Wu, Y. Chen, *RSC Adv.* **5**, 6494 (2015).
11. X. Huang, M. Wang, M. Willinger, L. Shao, D.S. Su, X. Meng, *ACS Nano* **6**, 7333 (2012).
12. W. Chen, H. Ruan, Y. Hu, D. Li, Z. Chen, J. Xian, J. Chen, X. Fu, Y. Shao, Y. Zheng, *CrystEngComm.* **14**, 6295 (2012).
13. Y.-C. Liang, C.-C. Wang, *RSC Adv.* **8**, 5063 (2018).
14. A. Sarkar, A.K. Singh, G.G. Khan, D. Sarkar, K. Mandal, *RSC Adv.* **4**, 55629 (2014).
15. Y.I. Choi, S. Lee, S.K. Kim, Y.-I. Kim, D.W. Cho, M.M. Khan, Y. Sohn, *J. Alloy. Compd.* **675**, 46 (2016).
16. Y. Wu, Y. Lin, J. Xu, *Photochem. Photobiol. Sci.* **18**, 1081 (2019).
17. M. Ahmad, H. Sun, A. Nisar, K. Maaz, G. Ali, S. Karim, *Nucleus* **4**, 180 (2015).
18. P. Basnet, D. Samanta, T.I. Chanu, J. Mukherjee, S. Chatterjee, *Mater. Res. Express* **6**, 085095 (2019).
19. P. Basnet, D. Samanta, T. Inakhunbi Chanu, J. Mukherjee, S. Chatterjee, *SN Appl. Sci.* **1**, 633 (2019).
20. A. Isaac, F. Sket, W. Reimers, B. Camin, G. Sauthoff, A.R. Pyzalla, *Mater. Sci. Eng. A* **478**, 108 (2008).